Journal of Alloys and Compounds 509 (2011) 5843–5847

Contents lists available at ScienceDirect

Journal of Alloys and Compounds

journal homepage: www.elsevier.com/locate/jallcom

Optical and Raman scattering studies on SnS nanoparticles

S. Sohila [a], M. Rajalakshmi [b,*], Chanchal Ghosh [c], A.K. Arora [b], C. Muthamizhchelvan [a]

[a] Centre for Material Science and Nano Devices, Department of Physics, SRM University, Kattankulathur, 603 203, Chennai, India
[b] Condensed Matter Physics Division, Indira Gandhi Centre for Atomic Research, Kalpakkam, 603102, India
[c] Physical Metallurgy Division, Indira Gandhi Centre for Atomic Research, Kalpakkam, 603102, India

ARTICLE INFO

Article history:
Received 8 October 2010
Received in revised form 11 February 2011
Accepted 24 February 2011
Available online 3 March 2011

Keywords:
Nanostructured materials
Semiconductors
Chemical synthesis
Optical properties
Phonons

ABSTRACT

Tin sulfide nanoparticles were synthesized through wet chemical route. Structure and phase purity were confirmed by powder XRD. Morphology and size were identified from TEM and AFM. The room temperature photoluminescence spectrum shows the band edge emission at 1.57 eV. The direct and indirect band gaps are estimated from UV–vis-NIR absorption spectrum as 1.78 and 1.2 eV, respectively. Blue shift of 0.48 eV observed for direct transition and 0.2 eV for indirect transition as compared to bulk band gap is due to quantum confinement effect. The Raman spectrum of SnS nanoparticles shows all the predicted Raman modes which show shift towards lower wave number side in comparison with those of the SnS single crystal. This is attributed to phonon confinement.

1. Introduction

In recent years there is considerable interest in semiconducting nanostructures owing to their optical and electrical properties being different from those of their bulk counterparts, due to the quantum confinement effect. Among the IV–VI group semiconductors, nanostructures of GeS, SnS and PbS are important materials. Research on SnS is attracted very much due to its layer property and being a less toxic compound compared to other similar materials such as lead and cadmium compounds. Tin sulfide is a narrow band gap IV–VI group semiconductor. SnS shows a variety of phases such as SnS, SnS_2, Sn_2S_3, Sn_3S_4 and Sn_4S_5 [1]. Among these compounds SnS has interesting properties and potential applications in the field of optoelectronic devices [2], absorber layer in thin film solar cells [3], near infra red detector [4], holographic recording systems [5], anode material in lithium ion batteries [6] and semiconductor sensors [7]. Tin sulfide is a layered semiconductor with orthorhombic structure [8]. The direct and indirect band gaps are ~1.3 and 1.0 eV, respectively [9]. SnS has both *p*-type and *n*-type conductivity depending on the departure of Sn stoichiometry from ideal and also it has high absorption coefficient of $10^4\ cm^{-1}$ [10].

Thin films of SnS have been deposited using electrochemical deposition [9], chemical deposition [11], thermal evaporation technique [12], plasma-enhanced chemical vapor deposition [13], spray pyrolytic deposition [14], chemical bath deposition [15] and electron beam evaporation [10]. Tin sulfide nanostructures have been synthesized using hydrothermal method, solvothermal method, microwave-irradiation and aqueous solution route [16–22]. Widely different values of direct and indirect gap in SnS thin films and nanostructures have been reported [16,23,24]. Indirect band gap of 1.1 eV has been reported in SnS quantum dots [24] however the evidence of direct band gap has not been reported. Zhao et al. [25] have observed two photoluminescence peaks in SnS nanoparticles which are assigned to defect peaks whereas the band gap luminescence from SnS nanoparticles has not been reported so far. Nikolic et al. [8] have reported the Raman spectra of single crystal SnS. Price et al. [26] have reported the Raman spectra of SnS thin film. Gou et al. [27] and Liu et al. [22] have reported the Raman spectra of SnS nanoparticles and nanowires, respectively wherein only a few Raman modes predicted by group theory have been observed. A detailed study comprising of the optical and vibrational properties of SnS nanoparticles in particular has not been reported. In the present work, we report the synthesis of SnS nanoparticles by wet chemical method and characterization done using AFM, TEM for size and morphology and XRD for phase identification, followed by detailed optical absorption, photoluminescence and Raman spectroscopic studies addressing the direct and indirect band gap transitions and all the predicted phonon modes in the SnS nanoparticles.

2. Experimental details

SnS nanoparticles were synthesized through wet chemical route. All the chemicals used in this work were of analytical grade and used without further purification.

* Corresponding author at: Condensed Matter Physics Division, Materials Science Group, Indira Gandhi Centre for Atomic Research, Kalpakkam, 603102, Tamilnadu, India. Tel.: +91 44 27480081; fax: +91 44 27480081.
E-mail address: Rajingmmsd@gmail.com (M. Rajalakshmi).

0925-8388/$ – see front matter © 2011 Elsevier B.V. All rights reserved.
doi:10.1016/j.jallcom.2011.02.141

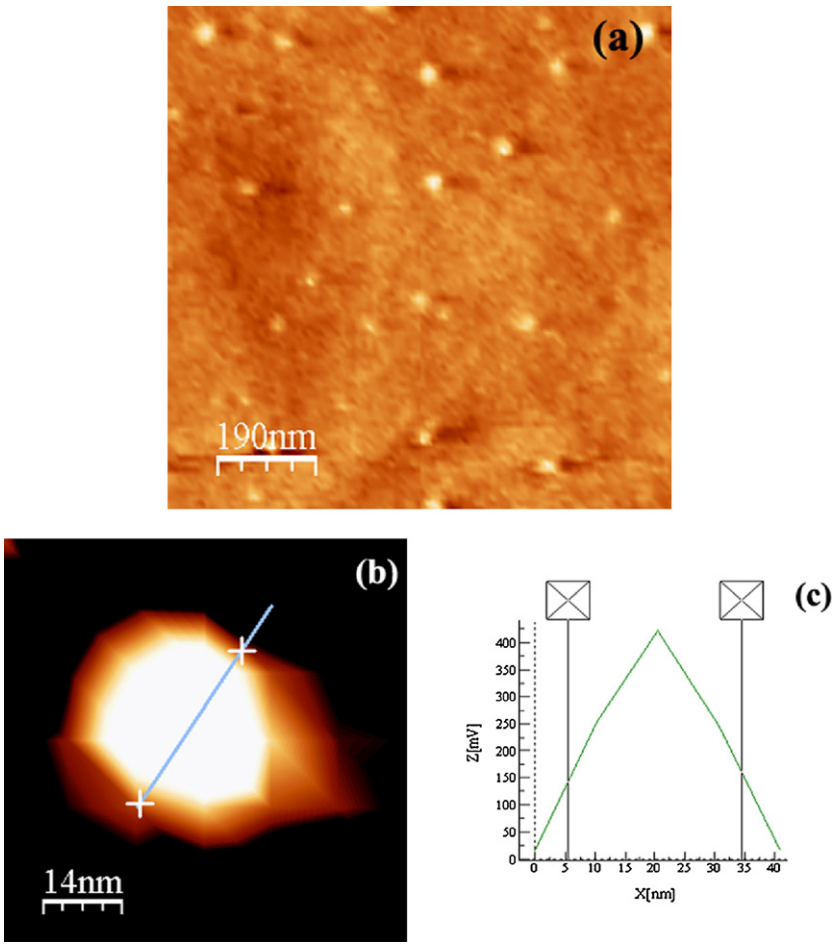

Fig. 1. (a) AFM image of SnS nanoparticles. (b) AFM image of SnS single nanoparticle. (c) Line profile of SnS nanoparticle.

Tin (II) chloride ($SnCl_2{\cdot}2H_2O$) and sodium sulfide (Na_2S) were taken as tin and sulfur sources, respectively. Appropriate amounts of tin (II) chloride and sodium sulfide solutions were used for precipitation. Sodium sulfide solution was added drop wise into the solution. The colorless tin (II) chloride solution turns dark brown color with the addition of sodium sulfide solution. This indicates the formation of SnS nanoparticles. This reaction was carried out at room temperature for 2 h. The precipitated particles were centrifuged and washed with deionised water and ethanol for several times. The final product was dried.

The phase purity of the synthesized sample was examined using STOE powder X-ray diffractometer using CuKα radiation (λ = 0.15418 nm). The morphology and particle size of the synthesized SnS nanoparticles were identified using Agilent Technologies' PicoLE Scanning Probe microscope (AFM), JEOL-2000 EX II high resolution transmission electron microscope operated at 200 kV. The optical absorption spectrum was recorded using Perkin Elmer Lamda 5 UV-visible spectrometer. Room temperature photoluminescence and Raman scattering measurements were carried out on the synthesized SnS nanoparticles. 325 nm laser line of He–Cd laser was used to excite photoluminescence and 532 nm line of diode – pumped solid – state laser was used to excite the Raman spectra. SPEX double monochromator was used to analyse the spectra and PMT was used as detector.

3. Results and discussion

AFM studies were carried out on the SnS nanoparticles. For this, SnS nanoparticles were coated on the silicon substrate by using spin coating method. Fig. 1(a) shows the AFM image of SnS nanoparticles coated on the silicon substrate. AFM image shows uniformly distributed spherical SnS nanoparticles. Size of SnS nanoparticles measured from AFM image is ~15 nm. Fig. 1(b) shows the single particle size and Fig. 1(c) shows the line profile.

Fig. 2(a) shows the bright field TEM micrograph of SnS nanoparticles. From the micrograph it is quite evident that the SnS nanoparticles are agglomerated among themselves. In due course of time the SnS nanoparticles are agglomerated due to the high surface energy which is shown in the TEM image. More polar solvents better wet the surface of the nanoparticles. The adsorption of polar solvents prevents the further growth of SnS nanoparticles but still the agglomeration of nanoparticles is taking place because of high surface energy [28]. Size of SnS nanoparticles measured from TEM image is varying from 7 to 15 nm. Fig. 2(b) shows the high resolution transmission electron micrograph (HRTEM) from a single SnS nanocrystallites and imaging the 0.324 nm spaced lattice fringes correspond to (0 2 1) plane of orthorhombic SnS. Fig. 2(c) shows the selected area electron diffraction (SAED) pattern from a region of the SnS nanoparticles. Phase identification was made from scaled SAED images by calculating the lattice spacing and then comparing with standard JCPDS values (39-0354).

Fig. 3 shows the powder XRD pattern of the sample. All the diffraction peaks are indexed to pure orthorhombic phase of SnS. This is in good agreement with the values of standard card (JCPDS NO 39-0354). The average particle size is calculated using Scherrer's formula as ~20 nm. This is due to agglomeration of the particles in the powder sample due to storage and hence XRD was used for phase identification only. Apart from SnS peaks, two additional peaks were seen in the XRD which are marked as * in XRD and are indexed to the impurity phase of β-Sn (JCPDS NO 04-0673) of very low level.

Optical absorption measurement was carried out on SnS nanoparticles. For this the nanoparticles were dispersed in ethanol. Fig. 4(a) shows the UV–visible-NIR absorption spectrum of SnS nanoparticles. For bulk SnS the direct band gap transition is at 1.3 eV and the indirect transition is at 1.0 eV, respectively. The dependence

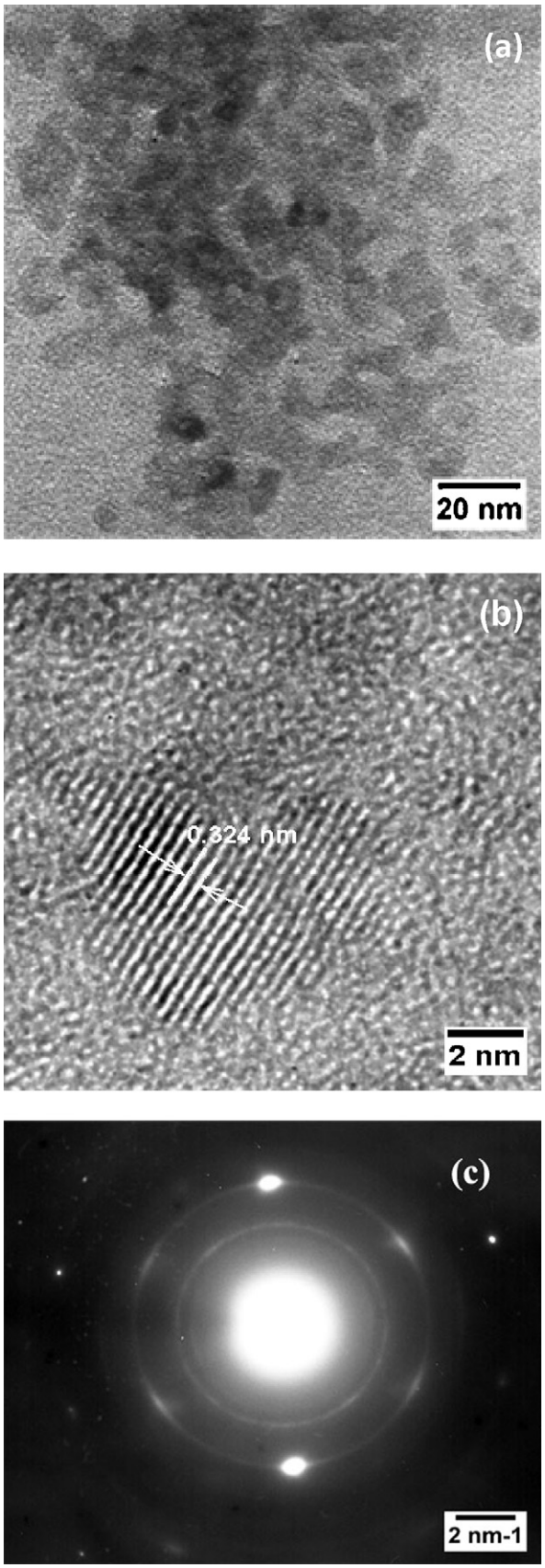

Fig. 2. (a) TEM image of SnS nanoparticles, (b) HRTEM image of SnS nanoparticles and (c) SAED image of SnS nanoparticles.

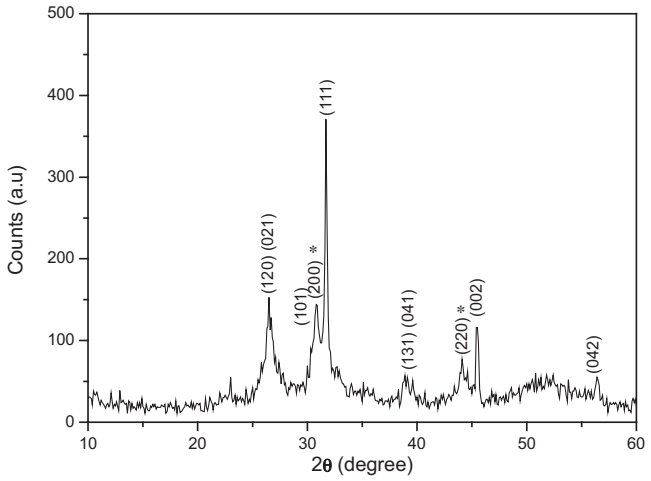

Fig. 3. Powder XRD pattern of SnS nanoparticles and the peaks labeled with *correspond to β-Sn.

of absorption coefficient (α) on the photon energy for semiconductors can be written as:

$$(\alpha h\upsilon)^n = B(h\upsilon - Eg)$$

where B is constant, n is the number that depends on the electronic transition [16]. The value of n is 2 and 1/2 for direct and indirect transition respectively. The dependence of α^2 on the photon energy ($h\upsilon$) and $(\alpha)^{0.5}$ on the photon energy ($h\upsilon$) for direct and indirect band gaps is shown in the Fig. 4(b) and (c), respectively. An estimate of direct and indirect band gaps from the intercept of plot is 1.78 and 1.2 eV, respectively. There are many reports with different values of direct and indirect gap in SnS thin films and nanostructures. For example, Zhu et al. have measured both direct and indirect band gaps for SnS nanoflowers from optical absorption spectrum as 1.53 and 1.43 eV, respectively [16]. Using optical absorption spectrum direct band gap of SnS films was reported as 1.92 eV [23] and for SnS quantum dots using DMEA as stabilizing agent the indirect band gap was reported as 1.1 eV [24]. In semiconductor nanoparticles the band gap is known to increase as the size is reduced. This arises due to quantum confinement of carriers [29]. A change in the band gap can also arise due to departure from ideal stoichiometry. The Bohr radius of SnS is 7 nm [30]. The diameter of the SnS nanoparticles is of the order of Bohr radius of SnS and hence the observed blue shift of 0.48 and 0.2 eV for direct and indirect transition, respectively is attributed to quantum confinement effect.

The room temperature photoluminescence (PL) spectrum was recorded using 325 nm He–Cd laser and Fig. 5 shows the PL spectrum of as synthesized SnS nanoparticles. The PL spectrum shows the emission peak at 12,680 cm^{-1} (1.57 eV). As mentioned earlier, bulk SnS has a direct gap of 1.3 eV and indirect gap of 1.0 eV. Hence the PL emission at 12,680 cm^{-1} can be attributed to the direct interband transition of SnS nanoparticles. This shows a blue shift of 0.27 eV compared to bulk SnS. This is in good agreement with the optical absorption results. Generally indirect transition does not result in PL emission.

Raman scattering measurements were carried out on SnS nanoparticles. Tin sulfide has orthorhombic structure with eight atoms per unit cell. For orthorhombic structure the 24 vibrational modes are represented by the following irreducible representations at the centre of Brillouin zone as:

$$\Gamma = 4A_g + 2B_{1g} + 4B_{2g} + 2B_{3g} + 2A_u + 4B_{1u} + 2B_{2u} + 4B_{3u}$$

Tin sulfide has 21 optical phonons of which 12 are Raman active modes ($4A_g$, $2B_{1g}$, $4B_{2g}$ and $2B_{3g}$), seven are infrared active modes ($3B_{1u}$, $1B_{2u}$ and $3B_{3u}$) and two are inactive ($2A_u$) [8].

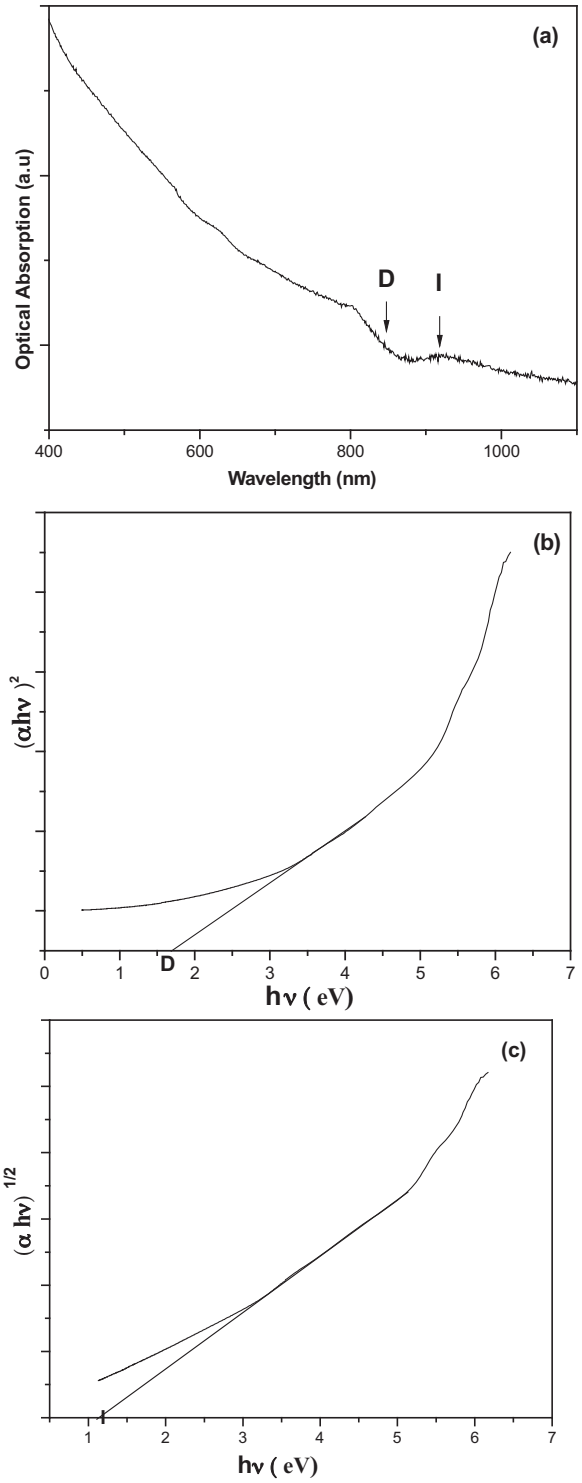

Fig. 4. (a) Optical absorption spectrum of SnS nanoparticles. D: direct transition, I: indirect transition, (b) Plot of $(\alpha h\upsilon)^2$ versus $h\upsilon$ showing direct band gap and (c) plot of $(\alpha h\upsilon)^{1/2}$ versus $h\upsilon$ showing indirect band gap of SnS nanoparticles.

Fig. 6 shows the room temperature Raman spectrum of SnS nanoparticles. The Raman modes for SnS nanoparticles are observed at 77, 109, 170, 182, 229 and 260 cm^{-1} along with some weak intensity modes at 46, 52, 57 and 154 cm^{-1}. Based on the previous report on Raman spectra of SnS single crystal, the observed Raman modes at 109 and 260 cm^{-1} are assigned to A_g mode and 77, 170 and 182 cm^{-1} are assigned to B_{2g} mode. We have observed a mode at 229 cm^{-1} and this mode is not observed in the Raman spectrum of SnS single crystal [8]. In accordance with Raman spectra of GeS, the Raman mode at 229 cm^{-1} is assigned to A_g mode [31]. We have observed a prominent B_{2g} mode at 182 cm^{-1} whereas in the case of single crystal spectra the intensity of B_{2g} mode at 194 cm^{-1} is weak. Also the intensity of the modes are prominent in the range of 40–60 cm^{-1} in the single crystal spectrum [8] whereas in the case of SnS nanoparticles the intensity of these modes are weak because of large background. This region of the spectrum is shown as an inset in the figure. The mode observed at 52 cm^{-1} is assigned to A_g mode and the modes at 57 and 154 cm^{-1} are assigned to B_{3g} mode. Table 1 compares the Raman modes in the present SnS nanoparticles with the single crystal data [8,31]. The Raman modes of SnS nanoparticles show broadening and are shifted towards lower wave number side as compared to Raman modes of SnS single crystal. This is due to phonon confinement effect. Liu et al. [22] have observed $2A_g$ modes at 223, 273.7 cm^{-1} and one B_{2g} mode at 190.4 cm^{-1} for SnS nanowires and Gou et al. [27] have observed only $2A_g$ modes at 189 and 220 cm^{-1} for SnS nanoparticles. For the SnS nanoparticles

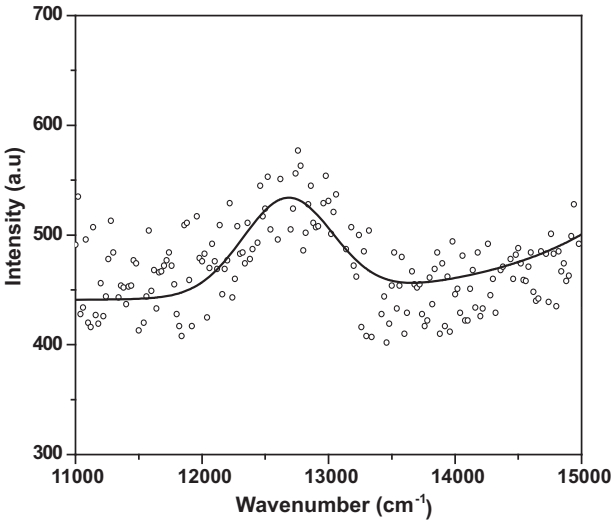

Fig. 5. Room temperature photoluminescence spectrum of SnS nanoparticles. The open symbols are experimental data and the solid curve is a Gaussian fit to the data.

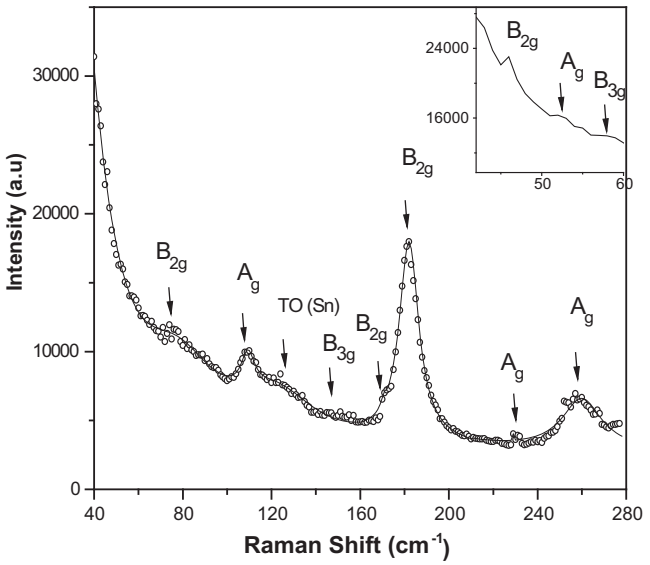

Fig. 6. Room temperature Raman spectrum of SnS nanoparticles. The open symbols are experimental data and the solid curve is a Lorentzian fit to the data. The insert shows the modes in the range from 40 to 60 cm^{-1}.

Table 1
Observed Raman modes of SnS nanoparticles.

A_g modes (cm^{-1})		B_{2g} modes (cm^{-1})	
SnS nanoparticles	SnS single crystal	SnS nanoparticles	SnS single crystal
109	111 [8]	46	47 [8]
229	238 [31]	77	78 [8]
260	264 [8]	170	170 [8]
		182	194 [8]

we have observed all the predicted Raman modes. A weak peak is observed at 124 cm^{-1} which does not belong to the predicted Raman modes of SnS. Pressure dependent Raman scattering studies on β-Sn showed LO and TO modes at 42.4 and 126.6 cm^{-1} at ambient pressure in which TO mode is prominent [32]. Based on this the mode observed at 124 cm^{-1} in our study can be assigned to TO mode of β-Sn since stoichiometric variations can lead to the presence of Sn in the system. However the intensity of this peak is weak suggesting the presence of small quantity of Sn in the system.

4. Conclusions

SnS nanoparticles were synthesized through wet chemical method. TEM and AFM showed the presence of spherical SnS nanoparticles of size in the range of 7–15 nm. The XRD pattern revealed the orthorhombic structure of SnS nanoparticles. The room temperature PL spectrum showed the band edge emission at 1.57 eV for direct transition. The estimated direct and indirect band gaps from optical absorption spectrum were 1.78 and 1.2 eV, respectively. A blue shift of 0.48 eV observed for direct transition and 0.2 eV for indirect transition compared to bulk band gap are due to quantum confinement. We have observed all the predicted Raman modes for the SnS nanoparticles from Raman scattering measurement. These modes were found to be shifted towards lower wave number side due to phonon confinement.

Acknowledgments

SS would like to thank SRM University for financial support and NanoTechnology Research Centre for AFM characterization. We thank Dr. R. Divakar, Mr. E. Mohandas for TEM characterization and Mrs. S. Kalavathi, Mr. V. Sankara Sastry for powder XRD measurements. We also thank Dr. B.V.R. Tata and Dr. C.S. Sundar for support and encouragement.

References

[1] T. Jiang, G.A. Ozin, J. Mater. Chem. 8 (1998) 1099–1108.
[2] N. Koteeswara Reddy, Y.B. Hahn, J. Appl. Phys. 101 (2007) 093522–093528.
[3] K.T. Ramakrishna Reddy, P. Purandhara Reddy, P.K. Datta, R.W. Miles, Thin Solid Films 403 (2002) 116–119.
[4] P. Pramanik, P.K. Basu, S. Biswas, Thin Solid Films 150 (1987) 269–276.
[5] M. Radot, Rev. Phys. Appl. 18 (1977) 345–351.
[6] G. Valiukonis, D.A. Guseinova, G. Krivaite, A. Sileica, Phys. Status Solidi B 135 (1990) 299–307.
[7] T. Jiang, G.A. Ozin, A. Verma, R.L. Bedard, J. Mater. Chem. 8 (1998) 1649–1656.
[8] P.M. Nikolic, P. Lj Miljkovic, B. Mihajlovic, Lavrencic, J. Phys. C: Solid Status Phys. 10 (1977) L289–L292.
[9] M. Ichimura, K. Takeuchi, Y. Ono, E. Arai, Thin Solid Films 98 (2000) 361–368.
[10] A. Tanusevski, D. Poelman, Sol. Energy Mater. Sol. Cells 80 (2003) 297–303.
[11] M. Ristov, Gj. Sinadinovski, I. Grozdanov, M. Mitreski, Thin Solid Films 173 (1989) 53–58.
[12] M.M.E.I. Nahass, N.M. Zeyada, M.S. Aziz, N.A.E.I. Ghamaz, Opt. Mater. 20 (2002) 159–170.
[13] A. Ortiz, J.C. Alonso, M. Garcia, J. Toriz, Semicond. Sci. Technol. 11 (1996) 243–247.
[14] B. Thangaraju, P. Kaliannan, J. Phys. D: Appl. Phys. 33 (2000) 1054–1059.
[15] A. Tanusevski, Semicond. Sci. Technol. 18 (2003) 501–505.
[16] H. Zhu, D. Yang, H. Zhang, Mater. Lett. 60 (2006) 2686–2689.
[17] S. Biswas, S. Kar, S. Chaudhuri, Appl. Surf. Sci. 253 (2007) 9259–9266.
[18] S.K. Panda, S. Gorai, S. Chaudhuri, Mater. Sci. Eng. B 129 (2006) 265–269.
[19] H. Peng, Li Jiang, J. Huang, G. Li, J. Nanopart. Res. 9 (2007) 1163–1165.
[20] D.S. Koktysh, J.R. McBride, S.J. Rosenthal, Nanoscale Res. Lett. 2 (2007) 144–148.
[21] Di Chen, G. Shen, K. Tang, S. Lei, H. Zheng, Y. Qian, J. Cryst. Growth 260 (2004) 469–474.
[22] Y. Liu, D. Hou, G. Wang, Chem. Phys. Lett. 379 (2003) 67–73.
[23] M. Devika, N. Koteeswara Reddy, M. Prashantha, K. Ramesh, S. Venkatramana Reddy, Y.B. Hahn, K.R. Gunasekhar, Phys. Status Solidi A 1 (2010), doi10.1002/pssa.200925379.
[24] Y. Xu, Najeh Al-Salim, C.W. Bumby, R.D. Tilley, J. Am. Chem. Soc. 131 (2009) 15990–15991.
[25] Y. Zhao, Z. Zhang, H. Dang, W. Liu, Mater. Sci. Eng. B 113 (2004) 175–178.
[26] L.S. Price, I.P. Parkin, A.M.E. Hardy, R.Z.H. Clark, T.G. Hibbert, K.C. Molloy, Chem. Mater. 11 (1999) 1792–1799.
[27] X.L. Gou, J. Chen, P.W. Shen, Mater. Chem. Phys. 93 (2005) 557–566.
[28] D. Heroux, A. Ponce, S. Cingarapu, K.J. Klabunde, Adv. Funct. Mater. 17 (2007) 3562–3568.
[29] L.E. Brus, J. Chem. Phys. 80 (1984) 4403–4409.
[30] G.H. Yue, L.S. Wang, X. Wang, Y.Z. Chen, D.L. Peng, Nanoscale Res. Lett. 4 (2009) 359–363.
[31] H.R. Chandrasekhar, R.G. Humphreys, U. Zwick, M. Cardona, Phys. Rev. B 16 (1977) 2981–2983.
[32] H. Olijnyk, Phys. Rev. B 46 (1992) 6589–6591.